

Analysis of photometric factors based on photometric linearization

Yasuhiro Mukaigawa,^{1,*} Yasunori Ishii,² and Takeshi Shakunaga²

¹*The Institute of Scientific and Industrial Research, Osaka University, 8-1 Mihogaoka, Ibaraki, Osaka 567-0047, Japan*

²*Department of Computer Science, Okayama University, 3-1-1 Tsushima Naka, Okayama 700-8530, Japan*

*Corresponding author: mukaigaw@am.sanken.osaka-u.ac.jp

Received January 3, 2007; revised May 30, 2007; accepted June 28, 2007;
posted August 2, 2007 (Doc. ID 78277); published September 24, 2007

We propose a method for analyzing photometric factors, such as diffuse reflection, specular reflection, attached shadow, and cast shadow. For analyzing real images, we utilize the photometric linearization method, which was originally proposed for image synthesis. First, we show that each pixel can be photometrically classified by a simple comparison of the pixel intensity. Our classification algorithm requires neither 3D shape information nor color information of the scene. Then, we show that the accuracy of the photometric linearization can be improved by introducing a new classification-based criterion to the linearization process. Experimental results show that photometric factors can be correctly classified without any special devices. A further experiment shows that the proposed method is effective for photometric stereo. © 2007 Optical Society of America

OCIS codes: 100.2960, 120.5700, 150.2950.

1. INTRODUCTION

The appearance of an object changes according to the lighting direction and surface reflectance. Since real images include complex factors such as specular reflections and shadows, it is difficult to apply some computer vision algorithms directly. For example, conventional photometric stereo [1] assumes a Lambertian surface without shadows. The shape-from-specularity method requires specular reflection regions, the shape-from-shadow method requires cast shadow regions, while bidirectional reflectance distribution function (BRDF) modeling requires separation of specular and diffuse reflections. It is therefore important to analyze the photometric factors included in real images.

Several methods have already been proposed for separating photometric factors. The dichromatic reflection model [2] is often used for separating diffuse and specular reflections [3–5]. These methods use color information to distinguish specular reflections from diffuse reflections. If the colors between light source and object are quite different, the clue is very powerful. However, if both colors are similar, the separation becomes difficult. Wolff and Boulton [6] proposed a method to separate specular reflections by analysis of reflected polarization, while Nayar *et al.* [7] combined color and polarization to separate specular reflections. Ikeuchi and Sato [8] proposed a method to classify photometric factors based on range and brightness images. These methods, however, have a common restriction in that shadows cannot be analyzed.

On the other hand, there are some methods that express real images in a linear subspace. Shashua [9] showed that an image illuminated from any direction can be expressed by a linear combination of three base images taken using different lighting directions assuming a Lambertian surface and a parallel ray. That is, an image can

be perfectly expressed in a 3D subspace. Belhumeur and Kriegman [10] showed that an image can be expressed by the illumination cone model even if the image includes attached shadows. In the illumination cone, images are expressed by a linear combination of extreme rays. Georgiades *et al.* [11] developed the illumination cone so that cast shadows can also be expressed by shape reconstruction. Although any photometric factor can ideally be expressed by the illumination cone, a large number of images corresponding to extreme rays are necessary.

We have proposed the photometric linearization method [12], which converts real images into ideal images that include only diffuse factors. After photometric linearization, all images are expressed as a linear combination of three base images. The method was originally proposed for image synthesis. In this paper, we show that the method can also be used for classifying photometric factors. It can classify not only diffuse and specular reflections, but also attached shadows and cast shadows. We present a new criterion for classification of photometric factors based on the photometric linearization. The classification algorithm requires neither 3D shape information nor color information of the scene. The classification is accomplished by a simple comparison of pixel intensities.

Moreover, we show that the accuracy of the original photometric linearization can be improved by introducing a new classification-based criterion to the linearization process. The original photometric linearization method does not work stably when pixels are not illuminated in a number of input images. Our physics-based analysis can solve this problem.

2. PHOTOMETRIC LINEARIZATION

We have proposed the photometric linearization method [12], which converts real images including various photo-

metric factors into ideal images, containing only diffuse reflection factors. First, we summarize the photometric linearization algorithm.

A. Photometric Factors

Photometric factors are classified into reflections and shadows as shown in Fig. 1. Reflections are further classified into diffuse reflections and specular reflections. According to the Lambert model, the intensity of the diffuse reflection is expressed by

$$i = \mathbf{n}^T \mathbf{s}. \quad (1)$$

Here, \mathbf{n} denotes the surface property vector, which is a product of the unit normal vector and the diffuse reflectance, and \mathbf{s} denotes the lighting property vector, which is a product of the unit vector along the lighting direction and the lighting power. Specular reflections are observed as the sum of diffuse factors and specular factors.

Shadows are classified into attached shadows and cast shadows. Attached shadows depend on the angle between the surface normal and the lighting direction and are observed where the angle between \mathbf{n} and \mathbf{s} is greater than 90° . Cast shadows depend on the overall 3D shape of the scene and are observed where light is occluded by other objects. If there is no ambient light or interreflection, the intensity of both shadows is zero.

B. Linearity of Diffuse Reflection

Shashua [9] showed that if a parallel ray is assumed, an image \mathbf{I}_k under any lighting direction can be expressed by a linear combination of three base images (\mathbf{I}_1 , \mathbf{I}_2 , and \mathbf{I}_3) taken using different lighting directions,

$$\mathbf{I}_k = c_k^1 \mathbf{I}_1 + c_k^2 \mathbf{I}_2 + c_k^3 \mathbf{I}_3. \quad (2)$$

Here, let $\mathbf{c}_k = [c_k^1 \ c_k^2 \ c_k^3]^T$ be a set of coefficients of the image \mathbf{I}_k .

C. Process Flow

Real images do not satisfy Eq. (2), because shadows and specular reflections are observed. The photometric linearization can convert real images, which include various photometric factors, into ideal images, which contain only diffuse reflection factors. That is, real images are converted into ideal images, which satisfy Eq. (1) perfectly. Since all pixels in the images fully satisfy Eq. (2) after the photometric linearization, any image can be expressed by a linear combination of three base images [9].

For the photometric linearization, multiple images are taken using different lighting directions. The camera and target objects are fixed. It is important that the lighting direction, the 3D shape of the target object, and the reflec-

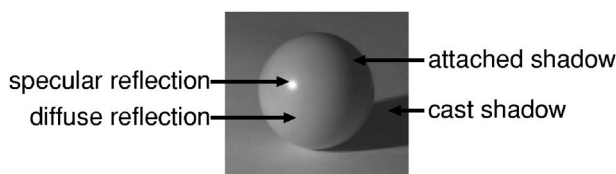


Fig. 1. Photometric factors included in an image.

tance of the surface are unknown. The process of photometric linearization is divided into the following three steps, as shown in Fig. 2:

1. Calculation of coefficients.
2. Photometric linearization of base images.
3. Photometric linearization of all input images.

Detailed algorithms are given in the following subsections.

1. Calculation of Coefficients

Let $\mathbf{I}_1, \mathbf{I}_2, \dots, \mathbf{I}_j$ denote the input images. First, three base images ($\mathbf{I}_1, \mathbf{I}_2, \mathbf{I}_3$), whose lighting directions are linearly independent, are selected from the input images. It is noted that the three base images should have large common regions of diffuse reflections. Although the selection affects the accuracy, the linearized result does not change.

The coefficients of the linear combination have to be determined to satisfy Eq. (2). If we calculate them by minimizing root mean square errors, correct coefficients cannot be calculated because of shadows and specular reflections. The photometric linearization solves this problem with the random sample consensus (RANSAC)-based approach. Many candidates are iteratively calculated by random sampling, and the correct value calculated from only diffuse reflections is selected from among the candidates. If all pixels are sampled from the diffuse reflection region, the correct value, which is not affected by specular reflections and shadows, is calculated. That is, we can regard the photometric linearization as a problem to find one correct value calculated using only diffuse reflection factors from among many candidates.

To calculate a candidate of the coefficients, three pixels are randomly selected from base images $\mathbf{I}_1, \mathbf{I}_2, \mathbf{I}_3$, and each input image \mathbf{I}_k . Note that the same pixels are selected from every image. A set of coefficients $\hat{\mathbf{c}}_k$ is calculated from the intensities of these pixels. If all the images include only diffuse components, unique coefficients are determined. By iterating this process, many candidate coefficients are obtained.

After iteration of this process, a coefficient distribution is obtained. If all the selected pixels include only diffuse

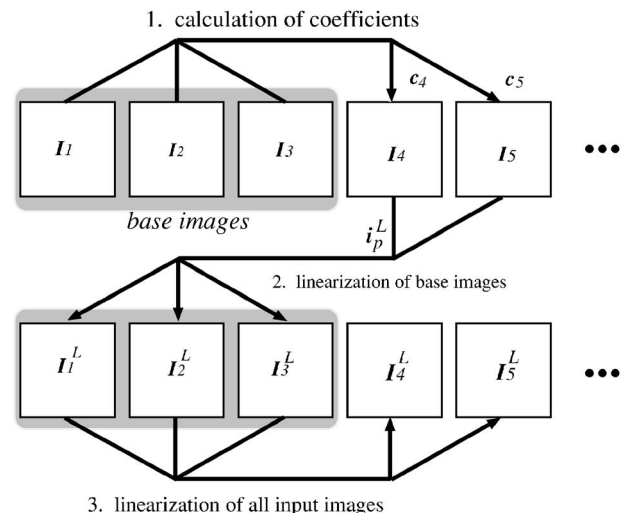


Fig. 2. Flow of the linearization process.

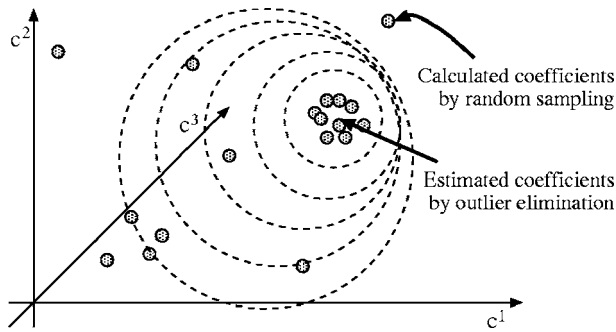


Fig. 3. Estimating the coefficients by random sampling and outlier elimination.

components, the calculated coefficients center around the correct point in the coefficient space in a dense formation as shown in Fig. 3. On the other hand, if the pixels include specular reflections or shadows, the coefficients are isolated from the correct point. Hence, the most reliable coefficients can be found by iterative calculation of a center of gravity and outlier elimination. The coefficients of the linear combination can be estimated reliably even if the input images contain specular reflections and shadows.

2. Photometric Linearization of Base Images

Next, we linearize the base images using the estimated coefficients for each input image. Three images ($\mathbf{I}_l, \mathbf{I}_m, \mathbf{I}_n$), excluding the three base images, are selected from the input images. Since the coefficients ($\mathbf{c}_l, \mathbf{c}_m, \mathbf{c}_n$) of the selected images have already been calculated, the base images ($\mathbf{I}_1, \mathbf{I}_2, \mathbf{I}_3$) can be regenerated by a linear combination of the selected input images and their coefficients.

If a pixel contains only a diffuse component in all the selected images, the pixel in the regenerated image also contains only a diffuse component. Although real images include other components, they are observed within a limited lighting direction for each pixel. Hence, an iterative method is used once again. The candidates for pixel intensity of the linearized base images are calculated by a linear combination of three input images which are selected at random. After iteration of the random selection and calculation, a pixel intensity distribution is obtained. The most reliable intensities are estimated in the same man-

ner as described in Subsection 2.C.1. As a result, the three base images $\mathbf{I}_1, \mathbf{I}_2$, and \mathbf{I}_3 are linearized to $\mathbf{I}_1^L, \mathbf{I}_2^L$, and \mathbf{I}_3^L , respectively.

3. Photometric Linearization of All Input Images

We have already obtained linearized base images ($\mathbf{I}_1^L, \mathbf{I}_2^L, \mathbf{I}_3^L$) and coefficients \mathbf{c}_k for each input image \mathbf{I}_k . All input images can now easily be linearized by linear combinations of the linearized base images with the coefficients. We denote the linearized \mathbf{I}_k as \mathbf{I}_k^L .

3. IMPROVEMENT OF PHOTOMETRIC LINEARIZATION

The photometric linearization was originally proposed for image synthesis. In this subsection, we show that the method can also be used for classifying photometric factors. We present a new criterion for classification of photometric factors based on the photometric linearization. Moreover, we show that the accuracy of the original photometric linearization can be improved by introducing a new classification-based criterion to the linearization process.

A. Criterion for Classification

In this subsection, we show that each pixel can easily be classified into diffuse reflection, specular reflection, attached shadow, and cast shadow based on the photometric linearization. The classification is accomplished by a simple comparison of the pixel intensity. That is, the classification does not need any additional information such as 3D shapes, lighting directions, or color information.

Let $i_{(k,p)}$ be the intensity of the pixel p in the image k , and let $i_{(k,p)}^L$ be the linearized intensity. The relationship between $i_{(k,p)}$ and $i_{(k,p)}^L$ is as follows: In the diffuse reflection region, $i_{(k,p)}^L$ is equal to $i_{(k,p)}$, because the intensity is not changed by the linearization. In the specular reflection region, $i_{(k,p)}^L$ is smaller than $i_{(k,p)}$, because the specular factor has been eliminated. Equation (1) indicates that the intensity in the attached shadow is negative, while that in cast shadow is positive. In the attached shadow region, $i_{(k,p)}^L$ becomes negative, which satisfies Eq. (1). In the cast shadow region, $i_{(k,p)}^L$ is larger than $i_{(k,p)}$, because $i_{(k,p)}^L$ has a diffuse reflection factor, while $i_{(k,p)}$ is near zero. Hence, each pixel can be classified by the following criterion:

$$\text{Region}(k,p) = \begin{cases} D: & \text{if } (|i_{(k,p)} - i_{(k,p)}^L| \leq T \times i_{(k,p)}) \cap (i_{(k,p)} \geq T_s) \\ S: & \text{if } (i_{(k,p)} - i_{(k,p)}^L > T \times i_{(k,p)}) \cap (i_{(k,p)}^L \geq 0) \cap (i_{(k,p)} \geq T_s) \\ A: & \text{if } (i_{(k,p)}^L < 0) \cap (i_{(k,p)} < T_s) \\ C: & \text{if } (i_{(k,p)}^L \geq 0) \cap (i_{(k,p)} < T_s) \\ U: & \text{otherwise} \end{cases} \quad (3)$$

Here, D , S , A , C , and U denote diffuse reflection, specular reflection, attached shadow, cast shadow, and an undefined factor, respectively. The threshold T is used to check the equality of $i_{(k,p)}$ and $i_{(k,p)}^L$, and is determined empirically. Since T is normalized to be relative to $i_{(k,p)}$, the check is independent of the brightness. In real images, the intensities of shadows are not zero. The threshold T_s is used to distinguish shadows, and can be determined by manually sampling some pixels in shadow regions.

In this criterion, the shadow regions are classified by only using threshold T_s . Although the classification is very simple, attached shadows and cast shadows can be distinguished by the sign of $i_{(k,p)}^L$. It is one of the significant advantages of the criterion because two types of shadows can be distinguished without any 3D shape information. Figure 4 illustrates Eq. (3) as a 2D plane spanned by $i_{(k,p)}$ and $i_{(k,p)}^L$. The photometric factors are easily classified once the photometric linearization has been accomplished.

B. Key Idea for Improvement

In Subsection 3.A, we showed that photometric factors are correctly classified if the photometric linearization is perfectly accomplished. That is, pixels are never classified as undefined factors. This fact suggests that the photometric linearization becomes more accurate by introducing the criterion for classification to the linearization process. We can use the criterion to verify the accuracy of the photometric linearization.

C. Introducing the Criterion for Classification

To find a correct value from the numerous candidates calculated by iterating the random sampling process, the previous method [12] iterates the estimation of the center of gravity and outlier elimination. However, the algorithm, which is based on the principle of majority, has weaknesses. Since the center of gravity may be affected by outliers, an incorrect candidate may be selected because of shadows. So the process tends to be unstable.

We now propose a new algorithm that can accurately determine the correct value from the many candidates. The distinction is based on the results of photometric classification. We check the photometric factors of all candidates, and therefore, introduce the criterion for classification into the photometric linearization process.

If a candidate is correct, each pixel is classified as one of the defined factors (D , S , A , and C) by Eq. (3). No pixel

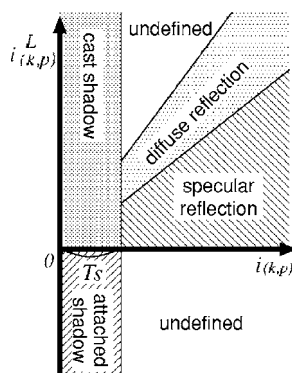


Fig. 4. Criterion for classification of photometric factors.

is ever classified as an undefined factor (U). Each candidate is evaluated according to the number of pixels, which are classified as the defined factors. The candidate that has the maximum number of pixels can be regarded as the correct value.

Essentially, the evaluation is based on the defined factors, with the exception of specular reflections. The specular reflection occupies a large area in Fig. 4. If we regard S as the defined factor, incorrect candidates may be accepted. Since the size of the specular region is relatively small in the images, we can ignore specular factors in this evaluation. Hence, we evaluate pixels that are classified as diffuse reflection, attached shadow, and cast shadow by

$$\text{Classifiable}(k,p) = \begin{cases} 1, & \text{if } (\text{Region}(k,p) = D \cup A \cup C) \\ 0, & \text{if } (\text{Region}(k,p) = S \cup U) \end{cases} \quad (4)$$

D. Evaluation of Candidates

In this section, we present the detailed algorithm to evaluate candidates. For each candidate $\hat{\mathbf{c}}_k$ of a set of coefficients, the k th input image \mathbf{I}_k is linearized to \mathbf{I}_k^L by the linear combination of the three base images \mathbf{I}_1 , \mathbf{I}_2 , and \mathbf{I}_3 . If $\hat{\mathbf{c}}_k$ is correct, Eq. (4) becomes one for almost all pixels. Hence, we define the following function to evaluate candidates of the coefficients $\hat{\mathbf{c}}_k$:

$$\text{Support}^C(k) = \sum_p \text{Classifiable}(k,p). \quad (5)$$

On the other hand, the linearized intensities $i_{(k,p)}^L$ are calculated by the linear combination using coefficients \mathbf{c}_k for each candidate $\hat{\mathbf{i}}_p^L$. If $\hat{\mathbf{i}}_p^L$ is correct, Eq. (4) becomes one for almost all input images. Hence, we define the following function to evaluate candidates of the linearized intensities:

$$\text{Support}^L(p) = \sum_k \text{Classifiable}(k,p). \quad (6)$$

These functions are used to calculate the number of pixels, which are classified as valid factors. $\text{Support}^C(k)$ is used when coefficients of the linear combination are calculated, and $\text{Support}^L(p)$ is used when the three base images are linearized. We can regard the candidate for which the function $\text{Support}^C(k)$ or $\text{Support}^L(p)$ returns the maximum, as the correct value. By using the estimated coefficients \mathbf{c}_k and intensities \mathbf{i}_p^L in the linearized base images, the accuracy of the photometric linearization can be improved.

E. Comparison with the Previous Method

It is noted that the proposed method takes the physical photometric phenomena into account, and considers the photometric factors of outliers, while the previous method [12] is based solely on the statistical framework. The accuracy can therefore be improved, especially in shadow regions.

One may think that if we simply modify [12] so that pixels below the threshold T_s are excluded as outliers, the accuracy can be improved. By ignoring dark regions, similar results may be acquired. However, the new method

can analyze the reason for shadows and classify them as either cast shadows or attached shadows. Shadows can thus be regarded as reasonable inliers.

4. EXPERIMENTAL RESULTS

We evaluated the proposed method using both synthetic and real images. For the experiments using real images, we used three kinds of materials with different reflection properties. A ceramic cup (Fig. 7) is an example of a rough glossy object, a pot (Fig. 11) is an example of a very shiny object, and a marble sphere (Fig. 12) is an example of complex reflection.

A. Evaluation Using Synthetic Images

To begin, we evaluated the proposed method numerically using synthetic images. The synthetic images were generated by POV-Ray, which is ray-tracing software. The scene contains a sphere and a cone as shown in Fig. 5. Twenty images were generated, using a different lighting direction for each.

Figure 6(a) shows the classification result using the proposed method, while Fig. 6(b) shows the result using the previous method [12]. Since this scene is artificially generated, we can easily generate no-shadow and no-highlight images. By comparison with such images, correct classification can be obtained as shown in Fig. 6(c). We call this result the “ground truth.” In the result of the previous method, some pixels of diffuse reflection are incorrectly classified as specular reflection. Obviously, the result of the proposed method is similar to the ground truth.

For the numerical evaluation, we count the number of pixels for each photometric factor in the ground truth image as shown in Table 1. We then check how accurately the pixels are classified based on the photometric linearization. Table 2 shows the classification results using the previous method and the proposed method, respectively. In the table, each row shows how accurately the correct photometric factor in the ground truth image is classified based on the photometric linearization. We can see that the proposed method can correctly distinguish cast shadow and attached shadow, as well as diffuse and specular reflection.

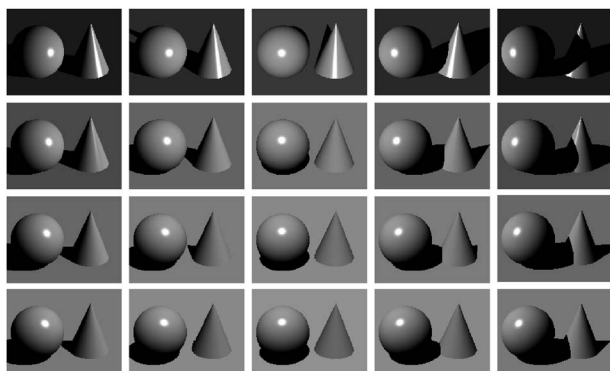


Fig. 5. Synthetic images.

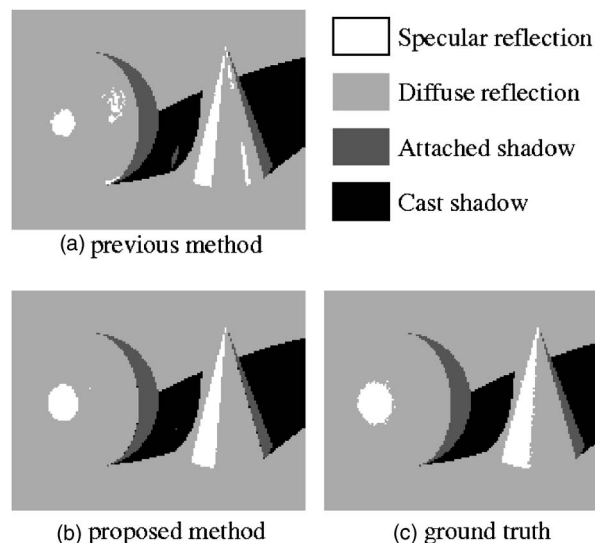


Fig. 6. Classification of photometric factors (synthetic scene).

B. Photometric Classification of Real Objects

We captured 24 images in a dark room using different lighting directions and keeping a halogen light away from the ceramic cup as shown in Fig. 7. Since this cup has a concave surface, some pixels are not illuminated in a number of the input images.

Figure 8 shows three base images selected from the input images; Fig. 8(a) shows the original base images, while Fig. 8(b) and 8(c) show the results of the photometric linearization. Since the linearized images have negative values, a zero level is expressed as a gray intensity. The results using the previous method are shown in Fig. 8(b). Many pixels are incorrectly linearized to be zero, because the previous method is strongly affected by cast shadows. The results of the new method based on the classification criterion are shown in Fig. 8(c). We can see that the base images are correctly linearized even if some pixels are not illuminated in a number of the input images.

Table 1. Number of Pixels for Each Photometric Factor

Photometric Factor	Number of Pixels
Cast shadow	2393
Attached shadow	845
Diffuse reflection	15007
Specular reflection	955

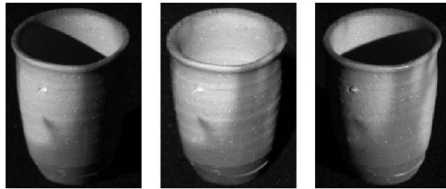
Table 2. Accuracy of the Classification (%)^a

		(a) Previous Method				(b) Proposed Method			
		C	A	D	S	C	A	D	S
C	99.04	0.96	0.00	0.00	C	99.96	0.04	0.00	0.00
A	0.00	100.00	0.00	0.00	A	1.78	98.22	0.00	0.00
D	0.00	0.00	99.01	0.99	D	0.00	0.00	99.99	0.01
S	0.00	0.00	43.56	56.44	S	0.00	0.00	17.49	82.51

^aC, cast shadow; A, attached shadow; D, diffuse reflection; and S, specular reflection.



Fig. 7. Input images taken using different lighting directions (cup: 24 images).



(a) three base images



(b) linearization by previous method



(c) linearization by proposed method

Fig. 8. Linearized base images.

Figure 9 shows the relationships between the intensities of the input images and the linearized images of a pixel corresponding to the inside of the cup. Figure 9(a) is

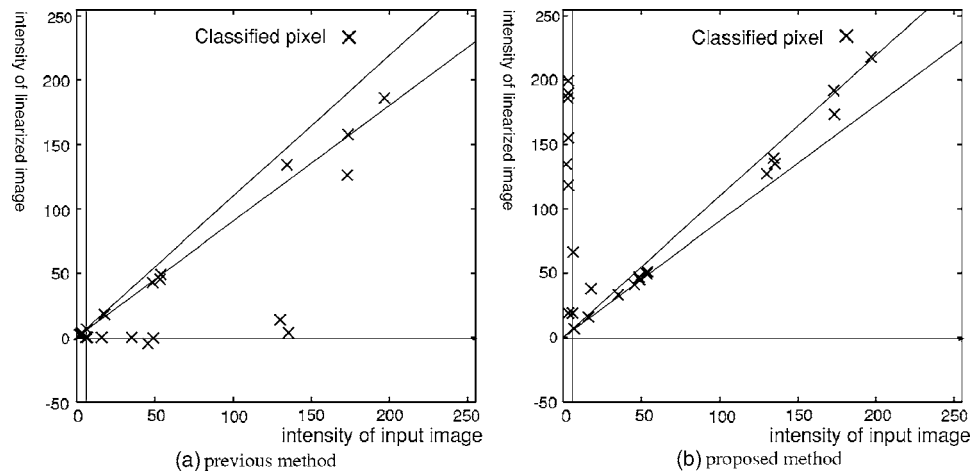


Fig. 9. Comparison of classification.

the result of the previous method and shows that many pixels on the inside of the cup are considered as dark surfaces without shadows. Some pixels are classified as an undefined factor. Figure 9(b) is the result of the proposed method and shows that almost all pixels are classified as one of the defined factors.

Figure 10 shows the results of the photometric classification. Figure 10(a) is an input image, while Fig. 10(b) is the linearized image. Comparing Figs. 10(a) and 10(b), each pixel is classified as Fig. 10(c) diffuse reflections, Fig. 10(d) specular reflections, Fig. 10(e) attached shadows, and Fig. 10(f) cast shadows. In these images, black pixels indicate the classified pixels. Although attached shadows and cast shadows cannot be classified by a simple threshold, the proposed method can distinguish them.

Some pixels on the inner side of the cup in Fig. 10(c) are incorrectly classified as diffuse reflection. These pixels should be classified as either attached shadow or cast shadow. The normal direction of these pixels is perpendicular to the lighting direction. Hence, it is difficult to distinguish dark diffuse reflection and attached shadow. The accuracy depends on the thresholds T and T_s .

Next, we applied our method to a glossy object with a complex shape. Figure 11(a) shows 24 images of the object. Figure 11(b) is the result of the photometric linearization. Figures 11(c)–11(f) show the results of the classification as diffuse reflections, specular reflections, attached shadows and cast shadows, respectively. Each pixel can be classified as a suitable photometric factor even if the target object has a complex shape.

C. Photometric Stereo

The conventional photometric stereo [1] assumes a Lambertian surface without shadows. There are, however, many improved algorithms for photometric stereo, such as the 4-source photometric stereo technique [13], which can recover surface normals in the presence of highlights and shadows. In this section, we show that the conventional simple photometric stereo method can easily be applied to a scene that includes highlights and shadows by combining our photometric linearization as a preprocess.

We captured 24 images of a marble sphere using different lighting directions (Fig. 12). Parts of the surface are

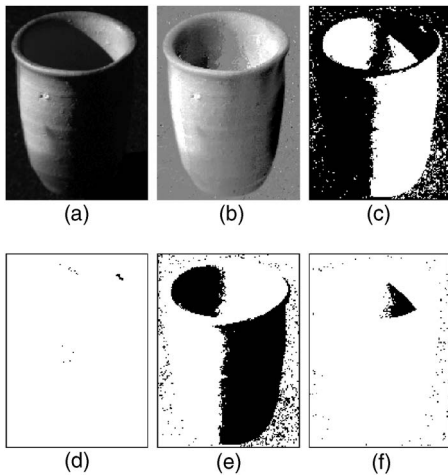


Fig. 10. Classification results of the photometric factors (cup). (a) Input image, (b) linearized image, (c) diffuse reflections, (d) specular reflections, (e) attached shadows, and (f) cast shadows. Black pixels indicate the classified pixels.

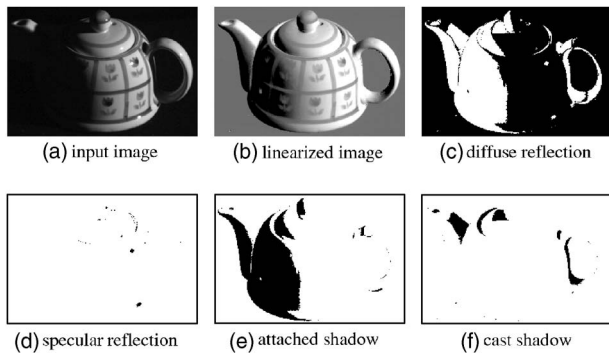


Fig. 11. Classification results of a glossy pot. Black pixels indicate the classified pixels.

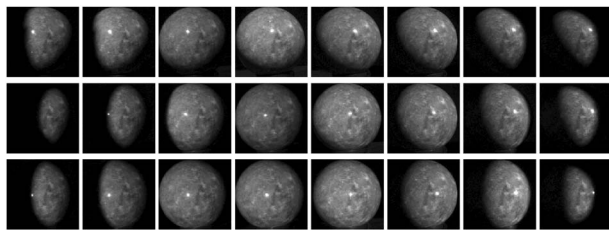


Fig. 12. Input images taken using different lighting directions (sphere).

not illuminated due to obstacles as shown in Fig. 13. First, all input images were linearized. The three selected base images and the linearized base images are shown in Figs. 14 and 15, respectively. Figures 15(a) and 15(b) show the results of the previous method and those of our method, respectively. The previous method failed in the linearization at the left- and right-hand sides of the sphere, because the pixels are not illuminated in a number of the input images due to shadows. On the other hand, our method is able to linearize the entire sphere correctly.

After the photometric linearization, the 3D shape was reconstructed by photometric stereo. Because the lighting directions are unknown, the surface normals cannot be uniquely determined in essentials [14]. In this experi-

ment, we know that the shape of the target object is a sphere. Hence, we sampled five points on the surface and calculated an affine transformation matrix by the least square method so that the surface normals correspond to those of the sphere. This process corresponds to estimation of the lighting direction using a known-shape object. Figure 16(a) is the ground truth shape obtained by manual measurement. Figures 16(b)–16(d) are the reconstructed shapes using the simple photometric stereo method, the previous method, and the proposed method, respectively. We can see that the simple photometric stereo method is affected by specular reflections, and the previous method fails in reconstruction at boundaries because of errors in the photometric linearization. On the other hand, the proposed method can correctly linearize and reconstruct the entire sphere. Table 3 shows the rms error and the largest error of the reconstructed 3D shape for each method. This result indicates that the photometric linearization is effective as a preprocess to the photometric stereo.

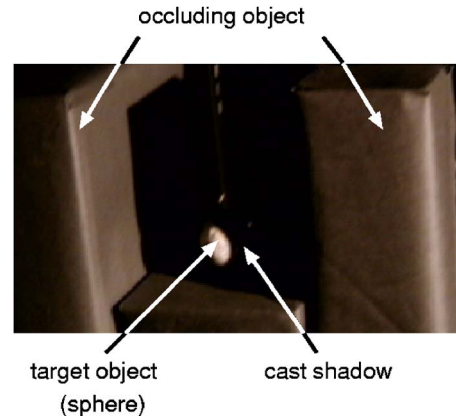


Fig. 13. (Color online) Target scene.

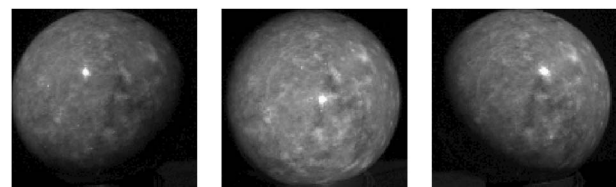
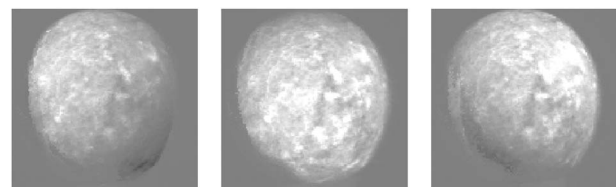


Fig. 14. Three selected base images.



(a) previous method



(b) proposed method

Fig. 15. Linearized base images.

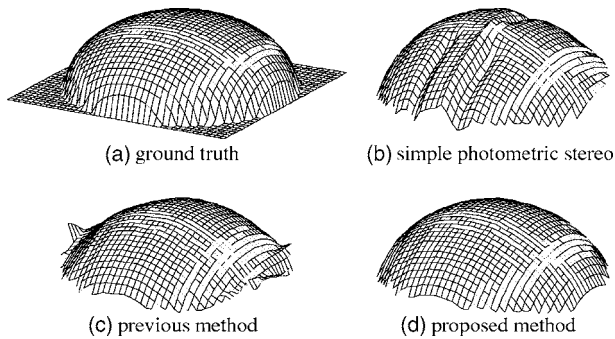


Fig. 16. Reconstructed 3D shapes.

Table 3. Comparison of Errors

Algorithm	Rms (mm)	Largest Error (mm)
Simple photometric stereo	5.11	14.41
Previous method	4.04	23.49
Proposed method	3.84	9.85

5. DISCUSSION

Real scenes include more complex illumination and reflection. In this section, we discuss the limitations of and extensions to the proposed method.

A. Specular Reflection on Rough Surface

In our algorithm, we assume sharp specular reflections on a glossy surface. This means that specular reflections are easily distinguished from diffuse reflection by a simple criterion as shown in Eq. (3) and that the number of specular reflection pixels are relatively small. Hence, we can regard the specular reflection as an undefined factor in Eq. (4).

If wide specular reflections are observed on a rough surface, the classification becomes more difficult because a part of the specular reflections may be included in the linearized images. In this case, other algorithms, for example those that use a polarizer [6] or color information [2,3], can be combined with our method.

B. Interreflection

Interreflection is an effect whereby reflected light on a surface illuminates the other surfaces again, and is observed at a concave part of an object. In our method, we assume that there is no interreflection.

Belhumeur and Kriegman have shown that interreflection on a Lambertian surface can also be expressed as a linear combination of three images [10]. This means that the interreflection effect will be included in the linearized image. Hence, the result of the photometric linearization cannot be used directly as a preprocess for the photometric stereo method. The relationship between the linearity of interreflections and the photometric linearization is under investigation.

C. Subsurface Scattering

Subsurface scattering is an effect of light transport in translucent materials, such as marble, skin, and milk. Since we assume opaque objects, our algorithm cannot be

applied to a material that has subsurface scattering. If strong subsurface scattering is observed, the linearity of the intensity cannot be satisfied.

In the experiment in Subsection 4.C, a marble sphere is used. Although subsurface scattering is observed on the sphere, the adverse effect is slight and thus, the photometric linearization succeeded.

D. Illumination

Our algorithm assumes a point light source at infinity. If there are multiple light sources or ambient light, the shadow cannot be classified correctly because shadow regions are found based on the threshold. Moreover, our algorithm assumes parallel light, and therefore a nearby point light source cannot be used. The extension to take complex illumination into consideration is one of our future works.

6. CONCLUSIONS

In this paper, we have proposed a new photometric classification method based on photometric linearization. While the photometric linearization was originally proposed for generating images using an arbitrary lighting direction, we showed that the method can also be used for the classification of photometric factors. We have improved the accuracy of the photometric linearization method by introducing the classification criterion into the linearization process.

The photometric linearization plays an important role as a fundamental technique of computer vision such as photometric stereo and shape-from-shading. We have confirmed that our method can be applied to a variety of materials, and that the photometric stereo becomes robust with respect to shadows by applying the photometric classification as a preprocess. In the future, we intend to analyze more complex factors such as interreflection.

ACKNOWLEDGMENTS

This research was partially supported by the Ministry of Education, Science, Sports and Culture, Grant-in-Aid for Young Scientists (A).

REFERENCES

1. R. J. Woodham, "Photometric stereo," MIT AI Memo (1978).
2. S. Shafer, "Using color to separate reflection components," *Color Res. Appl.* **10**, 210–218 (1985).
3. G. Klinker, S. Shafer, and T. Kanade, "The measurement of highlights in color images," *Int. J. Comput. Vis.* **2**, 7–32 (1988).
4. Y. Sato and K. Ikeuchi, "Temporal-color space analysis of reflection," *J. Opt. Soc. Am. A* **11**, 2990–3002 (1994).
5. Y. Sato, M. Wheeler, and K. Ikeuchi, "Object shape and reflectance modeling from observation," in *Proceedings of SIGGRAPH'97* (Association of Computing Machinery, 1997), pp. 379–387.
6. L. B. Wolff and E. Boulton, "Constraining object features using a polarization reflectance model," *IEEE Trans. Pattern Anal. Mach. Intell.* **13**, 635–657 (1991).
7. S. K. Nayar, X. Fang, and T. E. Boulton, "Removal of specularities using color and polarization," in *Proceedings*

- of the Conference on Computer Vision and Pattern Recognition '93* (IEEE, 1993), pp. 583–590.
8. K. Ikeuchi and K. Sato, “Determining reflectance properties of an object using range and brightness images,” *IEEE Trans. Pattern Anal. Mach. Intell.* **13**, 1139–1153 (1991).
 9. A. Shashua, “Geometry and photometry in 3D visual recognition,” Ph.D dissertation (Department of Brain and Cognitive Science, MIT, 1992).
 10. P. N. Belhumeur and D. J. Kriegman, “What is the set of images of an object under all possible lighting conditions?” in *Proceedings of the Conference on Computer Vision and Pattern Recognition '96* (IEEE, 1996), pp. 270–277.
 11. A. S. Georghiadis, D. J. Kriegman, and P. N. Belhumeur, “From few to many: illumination cone models for face recognition under variable lighting and pose,” *IEEE Trans. Pattern Anal. Mach. Intell.* **23**, 643–660 (2001).
 12. Y. Mukaigawa, H. Miyaki, S. Mihashi, and T. Shakunaga, “Photometric image-based rendering for image generation in arbitrary illumination,” in *Proceedings of the International Conference on Computer Vision 2001* (IEEE, 2001), pp. 652–659.
 13. S. Barsky and M. Petrou, “The 4-source photometric stereo technique for three-dimensional surfaces in the presence of highlights and shadows,” *IEEE Trans. Pattern Anal. Mach. Intell.* **25**, 1239–1252 (2003).
 14. P. N. Belhumeur, D. J. Kriegman, and A. L. Yuille, “The bas-relief ambiguity,” in *Proceedings of the Conference on Computer Vision and Pattern Recognition* (IEEE, 1997), pp. 1060–1066.